Nanoscale

http://www.paper.edu.cn
Dynamic Article Links

Cite this: *Nanoscale*, 2012, **4**, 3651

www.rsc.org/nanoscale

COMMUNICATION

Synthesis of micro-sized SnO_2@carbon hollow spheres with enhanced lithium storage properties

Shujiang Ding,[ab] Dongyang Zhang,[a] Hao Bin Wu,[b] Zhicheng Zhang[a] and Xiong Wen (David) Lou*[b]

Received 8th April 2012, Accepted 23rd April 2012
DOI: 10.1039/c2nr30841j

Uniform and stable micro-sized SnO_2 hollow spheres are prepared by templating against polystyrene microspheres. After being coated with a thin layer of amorphous carbon, the as-obtained SnO_2@ carbon hollow microspheres are shown to exhibit improved lithium storage properties, delivering a reversible capacity of 570 mA h g^{-1} after 50 cycles at a high current density of 400 mA g^{-1}.

Tin dioxide (SnO_2), usually regarded as an oxygen-deficient n-type semiconductor with a wide bandgap ($E_g = 3.6$ eV) and a rutile crystal structure,[1] has been widely investigated for numerous applications such as photocatalysis,[2] gas sensing,[3–5] supercapacitors,[6,7] and lithium-ion batteries (LIBs).[1,8–18] SnO_2 based nanocomposites are considered as promising anode materials for the next-generation LIBs because of the high theoretical capacity of SnO_2 (~790 mA h g^{-1}). However, the major barrier for SnO_2-based anode materials to replace the currently used graphite-based anode materials is the quick capacity fading upon extended charge–discharge cycling. This problem of SnO_2-based anode materials is believed to be related to the large volume variation during the repeated process of lithium uptake and release. One widely practiced strategy to effectively mitigate the above problem is to construct unique structures such as hollow,[1,8,12,19] mesoporous[20] or sheet-like[9,19] nanostructures, where the void spaces could buffer the volume change, leading to improved cyclic capacity retention. Another effective strategy is to make composites consisting of SnO_2 and carbon-based additives. Amorphous carbon,[21] carbon nanotubes[9,22,23] or graphene[10,14,24] are considered as good carbonaceous supports, since they can not only improve the electrical conductivity of the composite electrodes, but also provide a cushion effect against the internal stress induced by the volume change during the charge–discharge process.

Many nanostructures of SnO_2 have been synthesized using different methods. For example, we have previously synthesized SnO_2 hollow nanospheres based on a novel template-free hydrothermal method.[2] After that, a templating method using silica nanospheres has been developed to synthesize uniform SnO_2 hollow nanospheres with size in the range of 200–600 nm.[21] However, the same templating method using silica templates fails to produce micro-sized SnO_2 hollow spheres because of two factors: the relatively thin SnO_2 shell (20–30 nm) and the harsh silica-removal step involving HF or NaOH. In this work, we report an interesting approach to synthesize micro-sized SnO_2 hollow spheres by using sulfonated polystyrene (SPS) microspheres as the template. Importantly, the structure of the SnO_2 hollow spheres can be well preserved after the removal of the SPS microsphere template. Subsequently, the amorphous carbon coated SnO_2 hollow microspheres are obtained by hydrothermal deposition of a glucose-derived polysaccharide followed by carbonization at a moderate temperature under an inert atmosphere. The electrochemical measurements reveal that the as-prepared SnO_2@carbon hollow microspheres exhibit greatly improved lithium storage properties, which might be attributed to the larger cavity volume and thinner shell. Specifically, large cavity volume provides more empty space for buffering the volume variation of the electrode during the charge–discharge process and storing the electrolyte. The thin SnO_2 shell decreases the diffusion length of lithium ions.

The polystyrene microspheres are first treated with sulfuric acid,[25] prior to the deposition of the SnO_2 shell. We first examine the morphology of the SPS microspheres. From the field-emission

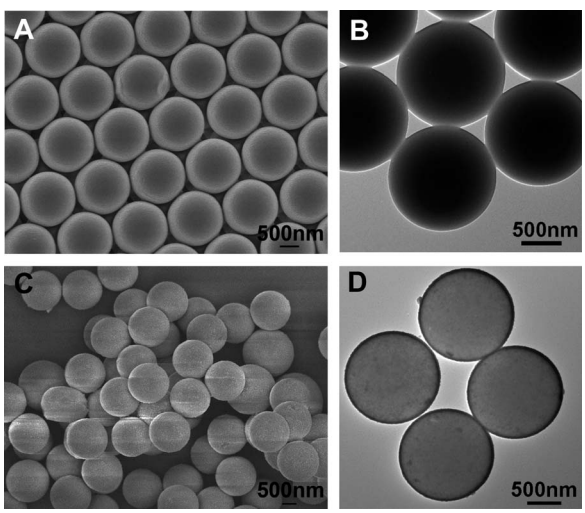

Fig. 1 (A) FESEM and (B) TEM images of SPS microspheres. (C) FESEM and (D) TEM images of SPS@SnO_2 core–shell microspheres.

[a]*MOE Key Laboratory for Nonequilibrium Synthesis and Modulation of Condensed Matter and Department of Applied Chemistry, School of Sciences, Xi'an Jiaotong University, Xi'an, P.R. China 710049. E-mail: dingsj@mail.xjtu.edu.cn*
[b]*School of Chemical and Biomedical Engineering, Nanyang Technological University, 70 Nanyang Drive, Singapore 637457. E-mail: xwlou@ntu.edu.sg*

scanning electron microscope (FESEM) image (Fig. 1A), it can be clearly observed that the SPS microspheres are very uniform with a diameter of about 1.4 μm. From the transmission electron microscopy (TEM) image (Fig. 1B), it is clear that the microspheres have a relatively smooth surface. After being coated with SnO_2, the surface becomes slightly rougher due to the presence of fine nanoparticles (Fig. 1C), indicating the successful deposition of the SnO_2 shell. The TEM image (Fig. 1D) shows that the shell has a thickness of about 30 nm. After being calcined in air, the SnO_2 hollow microspheres are obtained. The hollow interior can be directly observed through some small openings on the SnO_2 shells during the FESEM observation (Fig. 2A). The corresponding TEM image is shown in Fig. 2B, and the diameter of as-obtained SnO_2 hollow spheres is slightly reduced to about 1.3 μm, but the shell thickness increases to about 50–60 nm due to migration of some SnO_2 grown in the inner region of the SPS template onto the shell during thermal decomposition of the SPS template. After the carbon coating process, the diameter of obtained SnO_2@carbon hollow spheres is slightly increased (Fig. 2C and D). However it is hard to directly observe the carbon layer under TEM observation due to the relatively large size of the hollow spheres and the weak contrast of amorphous carbon.

The crystal structure of the SnO_2 hollow microspheres is determined by X-ray diffraction (XRD), as shown in Fig. 3A, curve I. All the identified peaks can be assigned to tetragonal SnO_2 (JCPDS card no. 41-1445, S.G.: $P4_2/mnm$, $a_o = 4.738$ Å, $c_o = 3.187$ Å). After the carbonization process at 500 °C for 2 h, the diffraction peak intensity increases significantly (Fig. 3A, curve II), suggesting the better crystallinity and larger crystallite size of the SnO_2 nanoparticles in the shell owing to the annealing. It should be noted that the carbon layer is amorphous and does not give rise to any diffraction peaks. Thermogravimetric analysis (TGA) is then employed to determine the carbon content in the SnO_2@carbon hollow microspheres and to study the thermal decomposition of the SPS microsphere template. Fig. 3B shows the weight losses of SPS@SnO_2 core–shell microspheres (curve I) and SnO_2@carbon hollow spheres (curve II). It can be seen from curve I that the decomposition of SPS takes place between 350 and 550 °C, and the polymer content is about 67.8 wt%. In curve II, the decomposition of carbon takes place between 350 and 500 °C, and the carbon content in the SnO_2@carbon hollow spheres

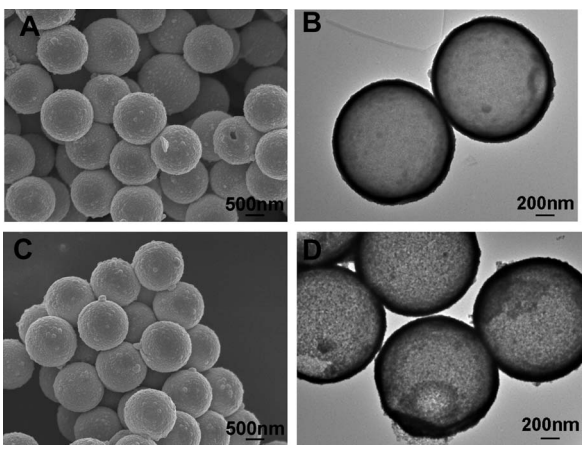

Fig. 2 (A) FESEM and (B) TEM images of the SnO_2 hollow microspheres. (C) FESEM and (D) TEM images of the SnO_2@carbon hollow microspheres.

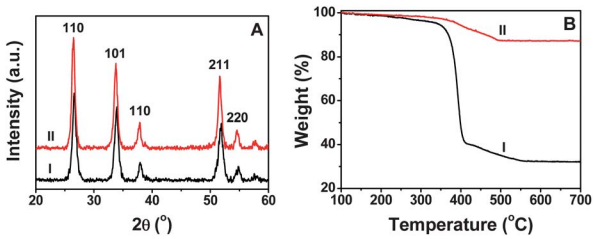

Fig. 3 (A) XRD patterns of SnO_2 hollow microspheres (I) and SnO_2@carbon hollow microspheres (II). (B) Thermogravimetric analysis (TGA) of SPS@SnO_2 microspheres (I) and SnO_2@carbon hollow microspheres (II).

can be calculated to be about 12.8 wt%. The Brunauer–Emmett–Teller (BET) specific surface area of these SnO_2@carbon hollow spheres is measured to be about 46 $m^2\ g^{-1}$.

Next, we investigate the electrochemical properties of SnO_2@carbon hollow microspheres as the anode material for LIBs. Fig. 4A shows the cyclic voltammograms (CVs) of the sample for the first, second, and fifth cycles. When SnO_2 serves as the active material in a Li/SnO_2 half-cell, the reaction mechanism can be described as follows:

$$SnO_2 + 4Li^+ + 4e^- \rightarrow Sn + 2Li_2O \quad (1)$$

$$Sn + xLi^+ + xe^- \leftrightarrow Li_xSn\ (0 \le x \le 4.4) \quad (2)$$

The CV curves are generally consistent with previous reports, indicating a similar electrochemical pathway.[1,12] The characteristic pair of peaks is observed in the first cycle at the cathodic and anodic potentials of 0.05 V and 0.7 V, respectively. These two peaks can be attributed to the alloying (cathodic sweep) and dealloying (anodic sweep) during charge–discharge processes, respectively, which contribute dominantly to the reversible lithium storage capacity by reaction (2). The peak appearing at 0.1–0.7 V is probably due to the reduction of SnO_2 to Sn by reaction (1). This reduction peak shifts to a higher voltage in the second cycle with a significant drop in the current intensity, giving rise to the broad peak at 0.6–1.4 V. This observation also suggests the partial reversibility of the reduction reaction (1) above. It can be noticed that the intensity of the anodic peak at 0.7 V in Fig. 4A increases during the second cycle, implying the existence of a possible activation process in the electrode material possibly because of the thin carbon layer. Generally, this sample demonstrates good reversibility of the electrochemical reactions, as only insignificant changes in the peak current and position can be observed after the second cycle.

Fig. 4B shows the discharge–charge voltage profiles of the SnO_2@carbon hollow microspheres at a constant current density of 400 mA g^{-1}. The voltage profiles are consistent with those of SnO_2-based anodes.[1,12] Interestingly, the as-prepared SnO_2@carbon hollow microspheres deliver a very high discharge capacity of 1557 mA h g^{-1} for the first cycle, with a corresponding charge capacity of ~595 mA h g^{-1}. This leads to an initial irreversible capacity loss of about 62%. This relatively high initial capacity loss is quite common for SnO_2-based electrode materials, and is mainly attributed to the irreversible reduction of SnO_2 to Sn as described by reaction (1) and other possible irreversible processes, such as the formation of the solid electrolyte interface (SEI).

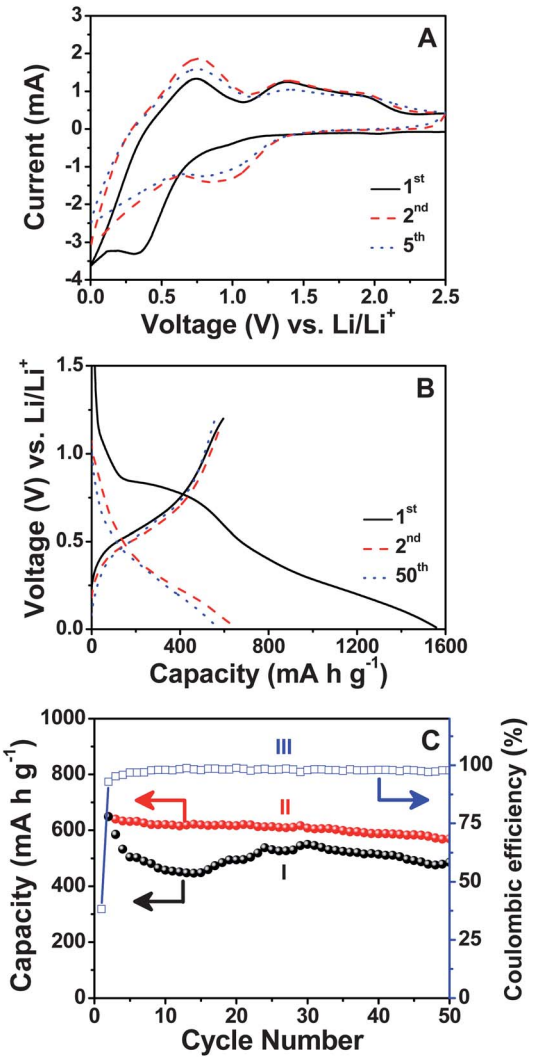

Fig. 4 Electrochemical characterizations of the SnO_2 and SnO_2@carbon hollow microspheres: (A) Cyclic voltammograms of SnO_2@carbon hollow microspheres (CVs) at a scan rate of 0.5 mV s^{-1} between 5 mV and 2.5 V. (B) Charge–discharge voltage profiles of SnO_2@carbon hollow microspheres. (C) Cycling performance of SnO_2 hollow microspheres (I) and SnO_2@carbon hollow microspheres (II) and the Coulombic efficiency (III). All charge–discharge measurements were conducted at a current rate of 400 mA g^{-1} between 0.01 V and 1.2 V.

Fig. 4C shows the cycling performance (curve II) and Coulombic efficiency (curve III) of SnO_2@carbon hollow microspheres with a voltage window of 0.01–1.2 V at a current density of 400 mA g^{-1}. At the end of 50 charge–discharge cycles, a reversible capacity as high as 570 mA h g^{-1} can be retained. It is much higher than that of pure SnO_2 nanoparticles (about 300 mA h g^{-1})[22] and SnO_2 hollow microspheres without a carbon coating (485 mA h g^{-1}, curve I). Even though the Coulombic efficiency is quite low in the first cycle, it quickly increases to 92.85% in the second cycle, and to 97.75% in the 50th cycle. We also investigate the cycling performance of SnO_2@carbon hollow microspheres at a current rate of 800 mA g^{-1}. At the end of 50 charge–discharge cycles, the reversible capacity is 493 mA h g^{-1}, which is slightly lower than 570 mA h g^{-1} at 400 mA g^{-1}. It is apparent that the as-prepared SnO_2@carbon hollow microspheres demonstrate much better lithium storage properties compared to the SnO_2 nanoparticles and SnO_2 hollow microspheres, in terms of both storage capacity and cyclic capacity retention.

In summary, we have demonstrated an efficient approach to synthesize uniform micro-sized SnO_2 hollow spheres with good structural stability using polystyrene microspheres as the template. After being coated with a thin layer of amorphous carbon, the as-prepared SnO_2@carbon hollow microspheres are shown to exhibit enhanced lithium storage properties compared to SnO_2 nanoparticles, delivering a reversible capacity of 570 mA h g^{-1} after 50 cycles at a high current density of 400 mA g^{-1}.

Experimental section

Materials synthesis

The polystyrene (PS) microspheres were prepared according to a previously reported method.[26] Then, the PS microspheres were decorated with $-SO_3H$ groups on the surface by treating with concentrated sulfuric acid to obtain sulfonated PS (SPS) microspheres.[25] In a typical synthesis of SPS@SnO_2 core–shell microspheres, 0.2 g of SPS microspheres was dispersed into 40 mL of 10 mM mercapto-acetic acid solution by ultrasonication for 5 min. Afterwards, 0.3 mL of concentrated hydrochloric acid, 0.5 g of tin(II) chloride dihydrate ($SnCl_2 \cdot 2H_2O$) and 0.5 g of urea were added into the above suspension. After stirring for 5 min, the reaction solution was transferred to a 150 mL flask and kept in an oil bath at 60 °C for 6 h under stirring. The precipitate was collected by centrifugation, washed thoroughly with ethanol, and dried at 80 °C for 12 h. The as-prepared SPS@SnO_2 core–shell microspheres were further treated at 450 °C in air for 2 h with a heating rate of 1 °C min^{-1} to obtain the highly crystalline SnO_2 hollow microspheres. In a typical synthesis of SnO_2@carbon composite hollow microspheres, 0.2 g of SnO_2 hollow microspheres was dispersed into 40 mL of 0.2 M glucose solution by ultrasonication for 10 min. The reaction solution was then transferred into a 60 mL Teflon-lined stainless steel autoclave and kept in an electric oven at 180 °C for 4 h. The autoclave was then taken out from the oven and left to cool down to room temperature. The black precipitate was collected by centrifugation, washed thoroughly with ethanol, and dried at 60 °C overnight. The product was treated at 500 °C under nitrogen for 4 h at a heating rate of 1 °C min^{-1} to obtain SnO_2@carbon hollow microspheres.

Materials characterization

The product morphology was examined using field-emission scanning electron microscope (FESEM; JEOL, JSM-6700F, 5 kV) and transmission electron microscope (TEM; JEOL, JEM-2100F, 200 kV). Crystallographic information of the samples was collected using powder X-ray diffraction (XRD; Bruker, D8 Advance X-ray diffractometer, Cu Kα radiation, λ = 1.5406 Å). The nitrogen sorption was performed using a Quantachrome Instrument (Autosorb AS-6B).

Electrochemical measurements

The electrochemical measurements were carried out using two-electrode Swagelok cells (X2 Labwares, Singapore) with a pure lithium foil as both the counter and the reference electrodes at room temperature. The working electrode consisted of an active material, a conductive agent (carbon black, Super-P-Li), and a polymer binder

(poly(vinylidene difluoride), PVDF, Aldrich) with a weight ratio of 70 : 20 : 10. The electrolyte used was 1.0 M $LiPF_6$ in a 50 : 50 (w/w) mixture of ethylene carbonate and diethyl carbonate. Cell assembly was carried out in an Ar-filled glove box with concentrations of moisture and oxygen below 1.0 ppm. Cyclic voltammetry (0.005–3.0 V, 0.5 mV s^{-1}) was performed using an electrochemical workstation (CHI 660C). The charge–discharge tests were performed using a NEWARE battery tester at a current rate of 400 mA g^{-1} with a voltage window of 0.01–1.2 V.

Acknowledgements

The authors are grateful to the National Research Foundation (Singapore) for financial support through the Clean Energy Research Programme (CERP; NRF2009EWTCERP001-036). Prof. S. Ding would like to thank the Fundamental Research Funds for the Central University.

Notes and references

1 X. W. Lou, Y. Wang, C. L. Yuan, J. Y. Lee and L. A. Archer, *Adv. Mater.*, 2006, **18**, 2325–2329.
2 Z. Liu, D. D. Sun, P. Guo and J. O. Leckie, *Nano Lett.*, 2006, **7**, 1081–1085.
3 X. Han, M. Jin, S. Xie, Q. Kuang, Z. Jiang, Y. Jiang, Z. Xie and L. Zheng, *Angew. Chem., Int. Ed.*, 2009, **48**, 9180–9183.
4 G. Xi and J. Ye, *Inorg. Chem.*, 2010, **49**, 2302–2309.
5 X. X. Xu, J. Zhuang and X. Wang, *J. Am. Chem. Soc.*, 2008, **130**, 12527–12535.
6 K. C. Ng, S. W. Zhang, C. Peng and G. Z. Chen, *J. Electrochem. Soc.*, 2009, **156**, A846–A853.
7 R. K. Selvan, I. Perelshtein, N. Perkas and A. Gedanken, *J. Phys. Chem. C*, 2008, **112**, 1825–1830.
8 X. W. Lou, L. A. Archer and Z. C. Yang, *Adv. Mater.*, 2008, **20**, 3987–4019.
9 S. J. Ding, J. S. Chen and X. W. Lou, *Adv. Funct. Mater.*, 2011, **21**, 4120–4125.
10 S. J. Ding, D. Y. Luan, F. Y. C. Boey, J. S. Chen and X. W. Lou, *Chem. Commun.*, 2011, **47**, 7155–7157.
11 J. Fan, T. Wang, C. Z. Yu, B. Tu, Z. Y. Jiang and D. Y. Zhao, *Adv. Mater.*, 2004, **16**, 1432–1436.
12 S. J. Han, B. C. Jang, T. Kim, S. M. Oh and T. Hyeon, *Adv. Funct. Mater.*, 2005, **15**, 1845–1850.
13 Y. Wang, H. C. Zeng and J. Y. Lee, *Adv. Mater.*, 2006, **18**, 645–649.
14 L. S. Zhang, L. Y. Jiang, H. J. Yan, W. D. Wang, W. Wang, W. G. Song, Y. G. Guo and L. J. Wan, *J. Mater. Chem.*, 2010, **20**, 5462–5467.
15 F. Han, L. W. Cui, L. M. Run and L. A. Hui, *J. Mater. Chem.*, 2012, **22**, 9645–9651.
16 S. J. Ding and X. W. Lou, *Nanoscale*, 2011, **3**, 3586–3588.
17 J. H. Kong, Z. L. Liu, Z. C. Yang, H. R. Tan, S. X. Xiong, S. Y. Wong, X. Li and X. H. Lu, *Nanoscale*, 2012, **4**, 525–530.
18 P. Wu, N. Du, H. Zhang, J. X. Yu, Y. Qi and D. R. Yang, *Nanoscale*, 2011, **3**, 746–750.
19 X. M. Yin, C. C. Li, M. Zhang, Q. Y. Hao, S. Liu, L. B. Chen and T. H. Wang, *J. Phys. Chem. C*, 2010, **114**, 8084–8088.
20 S. J. Ding, Z. Y. Wang, S. Madhavi and X. W. Lou, *J. Mater. Chem.*, 2011, **21**, 13860–13864.
21 X. W. Lou, C. M. Li and L. A. Archer, *Adv. Mater.*, 2009, **21**, 2536–2539.
22 S. J. Ding, J. S. Chen and X. W. Lou, *Chem.–Asian J.*, 2011, **6**, 2278–2281.
23 G. Chen, Z. Wang and D. Xia, *Chem. Mater.*, 2008, **20**, 6951–6956.
24 S. M. Paek, E. Yoo and I. Honma, *Nano Lett.*, 2009, **9**, 72–75.
25 S. J. Ding, C. L. Zhang, M. Yang, X. Z. Qu, Y. F. Lu and Z. Z. Yang, *Polymer*, 2006, **47**, 8360–8366.
26 S. J. Ding, B. Liu, C. L. Zhang, Y. Wu, H. F. Xu, X. Z. Qu, J. G. Liu and Z. Z. Yang, *J. Mater. Chem.*, 2009, **19**, 3443–3448.

